Disconnected entanglement entropy as a marker of edge modes in a periodically driven Kitaev chain

IOP Publishing Journal of Physics: Condensed Matter
J. Phys.: Condens. Matter **35** (2023) 085601 (15pp) https://doi.org/10.1088/1361-648X/aca7f7

Disconnected entanglement entropy as a marker of edge modes in a periodically driven Kitaev chain

Saikat Mondal[1,*], **Diptiman Sen**[2] **and Amit Dutta**[1]

[1] Department of Physics, Indian Institute of Technology, Kanpur 208016, India
[2] Centre for High Energy Physics and Department of Physics, Indian Institute of Science, Bengaluru 560012, India

E-mail: msaikat@iitk.ac.in

Received 7 September 2022, revised 7 November 2022
Accepted for publication 1 December 2022
Published 16 December 2022

Abstract

We study the disconnected entanglement entropy (DEE) of a Kitaev chain in which the chemical potential is periodically modulated with δ-function pulses within the framework of Floquet theory. For this driving protocol, the DEE of a sufficiently large system with open boundary conditions turns out to be integer-quantized, with the integer being equal to the number of Majorana edge modes localized at each edge of the chain generated by the periodic driving, thereby establishing the DEE as a marker for detecting Floquet Majorana edge modes. Analyzing the DEE, we further show that these Majorana edge modes are robust against weak spatial disorder and temporal noise. Interestingly, we find that the DEE may, in some cases, also detect the anomalous edge modes which can be generated by periodic driving of the nearest-neighbor hopping, even though such modes have no topological significance and not robust against spatial disorder. We also probe the behavior of the DEE for a kicked Ising chain in the presence of an integrability breaking interaction which has been experimentally realized.

Keywords: entanglement entropy, fermionic system, Floquet driving

(Some figures may appear in colour only in the online journal)

1. Introduction

There is a recent upsurge in studies of topological phases of matter [1–6]. These phases are robust against weak perturbations due to the existence of a bulk gap, which does not vanish unless the system crosses a gapless quantum critical point (QCP). In addition, a topological phase is characterized by a topological invariant, which remains constant under continuous variations of parameters as long as the system remains in the same phase and becomes ill-defined at QCPs which separate different phases.

In this regard, the Kitaev chain of spinless fermions (a p-wave superconducting system in one dimension) is a paradigmatic model that hosts symmetry protected topologically non-trivial and topologically trivial phases separated by a QCP [7, 8]. The topological properties of a Kitaev chain with periodic boundary conditions are characterized by a topological invariant known as the winding number. The winding number assumes non-zero integer-quantized values in the topologically non-trivial phase and vanishes in the topologically trivial phase. For a system with open boundary conditions, the topologically non-trivial phase of the model is manifested in the existence of zero-energy Majorana modes localized at the edges; on the contrary, the topologically trivial phase does not host Majorana edge modes. The exact solvability of the model

* Author to whom any correspondence should be addressed.

has been extensively exploited to understand its equilibrium as well as out-of-equilibrium properties [7–17].

Concerning the non-equilibrium dynamics of closed quantum systems, periodically driven systems have been explored both in the context of thermalization [18–30] and emergent topology [10, 11, 15, 17, 31–59] (for recent review articles, see references [17, 21, 26, 29]). For a periodically driven Kitaev chain with open boundary conditions, it has been shown that Majorana edge modes (zero and π-modes) can be dynamically generated [11, 15, 17] even though the instantaneous Hamiltonian may remain topologically trivial at all times. In fact, it is the effective Floquet Hamiltonian [60] that determines the non-trivial topology (i.e. the existence of Majorana edge modes) of a driven chain. It has been observed that the number of such dynamical edge modes increases as the drive frequency is reduced. Further, a strong (having a sufficiently large amplitude) periodic modulation of the hopping parameter can produce some 'anomalous' edge modes with non-zero Floquet quasienergies [15]. However, the anomalous edge modes are not Floquet Majorana modes. These modes have no topological significance and topological invariants like the winding number miss them completely. Furthermore, as we elaborate in this work, these modes are not robust against weak spatial disorder.

There have been several attempts to characterize the out-of-equilibrium topology of one-dimensional systems (for instance, the Kitaev chain and the Su-Schrieffer-Heeger chain) using the dynamical winding number calculated from the instantaneous wave function of the system [61–63]. In a periodically driven Kitaev chain, the corresponding winding number [11] is calculated from the Floquet Hamiltonian (for a review, see [17]). This winding number correctly predicts the number of the Floquet Majorana modes (zero modes and π-modes) for a Kitaev chain with a periodically driven chemical potential. However, the dynamical winding number fails to detect the anomalous edge modes which arise when the hopping parameter is driven strongly [15].

Recently, the notion of a disconnected entanglement entropy (DEE) [64–66] has been introduced which plays a role similar to a topological invariant in an equilibrium Kitaev chain with an open boundary condition. It is worth noting that unlike the winding number, the DEE is not a bulk topological invariant. Rather, it extracts the entanglement between the Majorana modes localized at the edges. Although the DEE can take any real value by its construction, it turns out to be integer-quantized for a short-ranged Kitaev chain in the topological phase, where the integer is the number of edge modes localized at each edge of the chain [64].

In this paper, we explore the efficacy of the DEE in detecting the dynamically generated edge modes for a periodically driven Kitaev chain. We study the variation of the DEE with the drive frequency for a periodic modulation of the chemical potential with δ-function pulses. Our study establishes that the DEE correctly predicts the number of Floquet Majorana edge modes. We also investigate the applicability of the DEE as a marker of anomalous edge modes appearing due to a periodic modulation of the nearest-neighbor hopping amplitude.

It is also noteworthy that the verification of topological properties of periodically driven systems are experimentally more viable compared to undriven systems. Recently, a periodically driven Ising model in the presence of an additional site-dependent random longitudinal field has been implemented experimentally using an array of superconducting qubits [67]. It is important to note that in the integrable limit (when the longitudinal field is absent), a transverse field Ising model can be mapped to a Kitaev chain through Jordan–Wigner transformation [68]. Although the Jordan–Wigner transformation is non-local, there is no non-local term consisting of long string operators in the Jordan–Wigner transformed Ising Hamiltonian with the open boundary conditions (unlike with the periodic boundary conditions) and thus it works fine with the open boundary conditions [69]. In the present work, we not only probe how these Floquet Majorana modes are manifested in the DEE, but also we illustrate the robustness of these modes against weak spatial disorder and temporal noise.

The rest of the paper is organized as follows: the conventional definition of the DEE is introduced in section 2. In section 3, we briefly recapitulate a short-ranged Kitaev chain of spinless fermions and its topological properties. The behavior of the DEE for a Kitaev chain with periodically modulated chemical potential is explored in section 4. We analyze the effects of spatial disorder and temporal noise in the periodic driving on the DEE in section 5. In section 6, we study the situation where the nearest-neighbor hopping amplitude is periodically modulated and address the question of whether the DEE can detect the anomalous edge modes. In section 7, probing the DEE, we analyze the robustness of the Floquet Majorana modes against an integrability breaking interaction in a periodically driven Ising model, as studied experimentally in [67]. Concluding remarks are presented in section 8. The definition of the winding number of a short-range (static) Kitaev chain is given in appendix A. The methods used for computing the DEE from Floquet Hamiltonian are explained in appendix B. We then briefly compare the DEE with the dynamical winding number derived from the Floquet Hamiltonian for a periodic variation of the chemical potential in appendix C. In appendix D, we provide an analytical derivation of the frequencies at which Floquet quasienergy gap becomes zero or $\pm\pi/T$, choosing the examples of a periodic driving of the hopping amplitude and an experimentally relevant driving protocol (discussed in section 7) for an Ising chain.

2. DEE

In this section, we briefly introduce the notion of DEE [64, 65]. To this end, we first consider a composite system $\mathcal{S}$ that is in a pure state and is described by a density matrix ρ. The reduced density matrix of a subsystem A is obtained by tracing over the degrees of freedom of the rest of the system $\overline{A}$ [70]:

$$\rho_A = \mathrm{Tr}_{\overline{A}}(\rho). \tag{1}$$

The entanglement entropy [71–74] of subsystem A is then defined in terms of the eigenvalues λ_i of the reduced density matrix ρ_A as

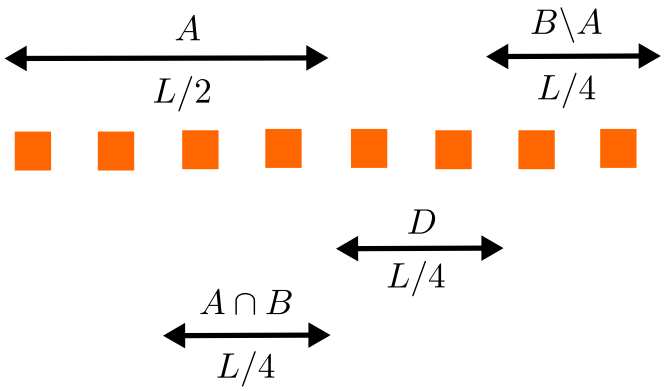

Figure 1. Partitions of a chain with the disconnected partition $D = \overline{A \cup B}$ and $2\ L_A = 2\ L_B = 4\ L_D = L$. The subsystem B consists of two partitions $A \cap B$ and $B \backslash A$, separated by the disconnected partition D. (In this figure, each square represents a fermionic site.).

$$S_A = -\mathrm{Tr}_A(\rho_A \ln(\rho_A)) = -\sum_i \lambda_i \ln(\lambda_i). \tag{2}$$

As the system $\mathcal{S}$ is in a pure state, it can be shown that $S_A = S_{\overline{A}}$.

We now consider a configuration of the partitions A, B, $A \cap B$ and $A \cup B$ of the system $\mathcal{S}$, such that the subsystem B consists of two parts $A \cap B$ and $B \backslash A$, separated by the disconnected partition $D = \overline{A \cup B}$, as shown in figure 1. The DEE [64–66] is then defined as

$$S_D = S_A + S_B - S_{A\cup B} - S_{A\cap B}. \tag{3}$$

3. Short-range Kitaev chain

We recall the Hamiltonian of a Kitaev chain [7–11] with short-ranged couplings given by

$$H = -\gamma \sum_{n=1}^{L-1} (c_n^\dagger c_{n+1} + c_{n+1}^\dagger c_n) - \mu \sum_{n=1}^{L} (2\, c_n^\dagger c_n - 1) + \Delta \sum_{n=1}^{L-1} (c_n c_{n+1} + c_{n+1}^\dagger c_n^\dagger), \tag{4}$$

where c_n ($c_n^\dagger$) is the annihilation (creation) operator for a spinless fermion on the nth site, γ is the nearest-neighbor hopping parameter, Δ is the strength of the p-wave superconducting pairing, and μ is the on-site chemical potential. The parameters γ, Δ and μ will be taken to be real unless otherwise mentioned. Consequently, the Hamiltonian respects time-reversal symmetry, particle-hole symmetry and sub-lattice/chiral symmetry and the system belongs to the BDI symmetry class [11, 12]. Definition of the winding number and topological properties of a short-range Kitaev chain are briefly discussed in appendix A.

It is noteworthy that in a chain with short-ranged couplings and open boundary conditions, the DEE, calculated in the ground state of static Hamiltonian, is an integer multiple of $\ln(2)$, i.e. $S_D = p \ln(2)$, where p is the number of modes localized at each edge of a chain with the open boundary conditions (see [64]). Therefore, the values of the DEE in the topologically non-trivial ($-1 < \mu < 1$) and trivial ($|\mu| > 1$) phases of a Kitaev chain with $\gamma = 1$ and $\Delta \neq 0$ are $\ln(2)$ and zero, respectively, and there is a discontinuous jump in the value of the DEE at the QCP separating the two phases. Thus, the DEE plays a role equivalent to the winding number for an open chain.

4. DEE for a Kitaev chain with periodically modulated chemical potential

In this section, we discuss the behavior of the DEE calculated in the ground state of the effective Floquet Hamiltonian for a Kitaev chain with a periodically modulated chemical potential.

We consider a Kitaev chain with an open boundary condition in which the chemical potential is periodically modulated [11], such that $\mu(t) = \mu(t+T)$, with $T = 2\pi/\omega$, where ω is the driving frequency, so that $H(t)$ in equation (4) satisfies $H(t) = H(t+T)$. For a time-periodic Hamiltonian $H(t)$, the stroboscopic time-evolution operator (i.e. the Floquet operator) is defined as

$$U_\mathrm{F} = \mathbb{T} \exp\left(-i \int_0^T H(t) dt\right) = \exp(-i H_\mathrm{F} T), \tag{5}$$

where H_F is the Floquet Hamiltonian and $\mathbb{T}$ denotes time-ordering. (We will set $\hbar = 1$ in this paper).

We recall that due to the unitary nature of the Floquet operator U_F, its eigenvalues are phases. Further, these appear in complex conjugate pairs, $e^{i\theta}$ and $e^{-i\theta}$ (see appendix B for details) because of particle-hole symmetry (as the system belongs to Floquet BDI symmetry class [11]). If present, Majorana edge modes correspond to the eigenvalues $+1$ and -1 of the Floquet operator (U_F). In other words, their corresponding Floquet quasienergies are $\epsilon_\mathrm{F} = 0$ and $\epsilon_\mathrm{F} = \pm\pi/T$, respectively. Thus, the total number of Majorana edge modes (twice the number of Majorana modes at each edge) is given by the total number of eigenvalues $+1$ and -1 of U_F.

We now consider the protocol in which the chemical potential μ is periodically modulated by the application of δ-pulses such that [11, 17]

$$\mu(t) = \mu_0 + \mu_1 \sum_{m=-\infty}^{\infty} \delta(t - mT), \tag{6}$$

where $T = 2\,\pi/\omega$. Both ω and μ_0 are in the units of the hopping parameter γ, where we have set $\gamma = 1$. On the other hand, the parameter μ_1 is dimensionless.

The chemical potential $\mu(t)$ in equation (6) for a Kitaev chain can be mapped to a transverse field in an Ising chain through the Jordan–Wigner transformations [68]. If the transverse field of an Ising chain is periodically kicked (with δ-function kicks), then the driving protocol of the quantum Ising chain can be mapped to the driving protocol as in equation (6). It is noteworthy that a quantum Ising model can be simulated with quantum circuits [75] and δ-function kicks can be experimentally realized with laser pulses [76].

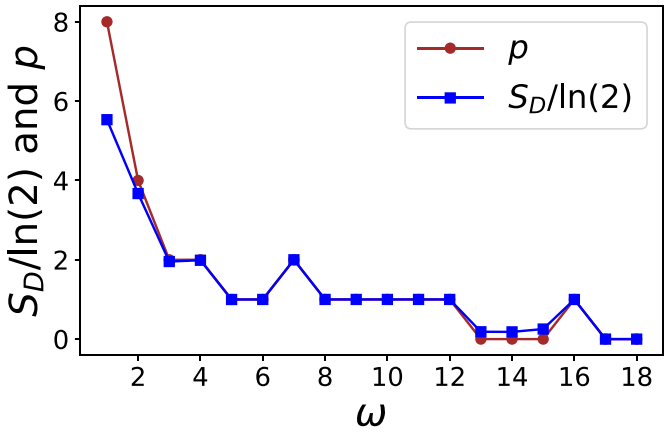

Figure 2. DEE (S_D) in units of $\ln(2)$ and the number of Majorana edge modes (p) localized at each edge as functions of driving frequency ω (in the units of the hopping parameter γ, which is set equal to unity) for a Kitaev chain in which the chemical potential μ is periodically modulated by δ-pulses (equation (6)) with $\mu_0 = 2.5$ and $\mu_1 = 0.2$. We have taken $\Delta = 1$, $L = 200$ and $L_D = 50$. Here, both the parameters μ_0 and Δ are in the units of γ, while the parameter μ_1 is dimensionless. The DEE assumes integer-quantized values except at low frequencies. The number of dynamically generated edge Majorana modes increases as ω decreases.

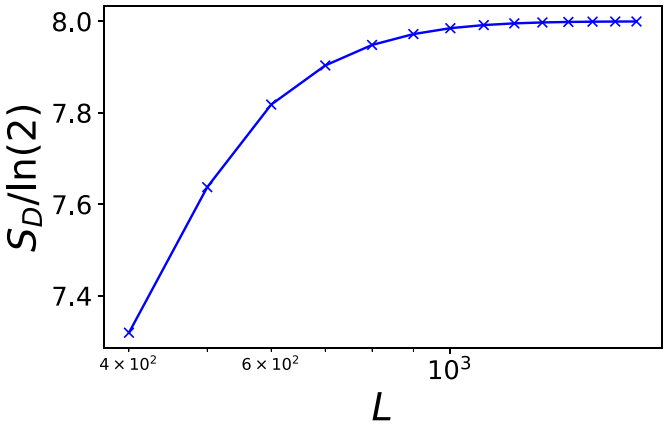

Figure 3. DEE (S_D) in units of $\ln(2)$ as a function of the length L (in semi-log scale) of a Kitaev chain (with $L_D = L/4$) in which the chemical potential μ is periodically modulated by δ-pulses (equation (6)) with $\mu_0 = 2.5$, $\mu_1 = 0.2$, $\Delta = 1$ and $\omega = 1$. Here, μ_0, ω and Δ are in the units of γ, while the parameter μ_1 is dimensionless. We observe a saturation to an integer-quantized value as L increases, establishing that the discrepancy observed for low ω in figure 2 is a finite-size effect.

We now calculate the DEE in the ground state of the Floquet Hamiltonian H_F for this driving protocol in a Kitaev chain with open boundary conditions. The methods used to calculate the DEE from the correlation matrix are explained in appendix B. In this driving protocol, the DEE, calculated in the ground state of the Floquet Hamiltonian, is equal to integer multiples of $\ln(2)$, as can be seen from figure 2. Thus, $S_D = p\ln(2)$, where p is an integer. It is also interesting to note that the DEE generally increases as the drive frequency ω decreases. Further, we have verified that the value of $S_D/\ln(2)$ is equal to the number of Majorana edge modes (both zero and π-modes) localized at each edge of the chain (see figure 2) generated by the same periodic driving of the Kitaev chain.

However, at low drive frequencies (i.e, when ω is of the order of the hopping parameter γ), the DEE is not integer-quantized and the value of $S_D/\ln(2)$ differs significantly from the number of Majorana end modes. This is however a finite-size effect, as shown in figure 3, which demonstrates that the DEE does saturate to an integer-quantized value for large system size L. The reason for the finite-size effect is that at low frequencies, the decay lengths of the Majorana edge modes increase and therefore the edge modes mix more and more with the bulk states. In other words, the average normalized participation ratio (NPR) for the edge-modes is of the order of unity at low drive-frequencies [55], while the NPR is of the order of $1/L$ when the frequency is not sufficiently low [55]. (For a normalized wave function $\psi_j(n)$, where j labels the eigenstate and n denotes the site index, the participation ratio is defined as $R_j = 1/(\sum_n |\psi_j(n)|^4)$ and the average NPR [55] is defined as, NPR$= \langle R_j\rangle/L$, where the average is taken over all the eigenstates. The average NPR is of the order of unity and $1/L$ for extended states and localized states, respectively [55]). When the decay length is comparable to the size $L/4$ of the disconnected region D, the contribution of such end modes to the DEE deviates from integer multiples of $\ln(2)$ (i.e. the DEE fails to detect these edge-modes correctly). This leads to the reduction in the contribution of the edge-modes to the DEE. On the other hand, at low frequencies, the bulk states become long-range entangled (as the effective range of couplings appearing in the Floquet Hamiltonian increases with decreasing drive frequency) and the long-range entangled bulk states contribute to the DEE (see [66]). This effect leads to an increase in the DEE. For small ω, therefore, the deviation of the DEE from integer-quantized value occurs due to the competition between these two contradictory effects. As the length $L_D = L/4$ is increased, the bulk contribution to the DEE decreases [66]. Also, with the increase of L, the dispersion of the edge modes to the bulk states decreases (as the decay lengths of the Floquet Majorana modes are much smaller than the system-size L, when L is sufficiently large), even at low drive frequencies. Thus, for sufficiently large L (and therefore sufficiently large $L_D = L/4$), the bulk contribution becomes negligibly small and the DEE only contains the integer-quantized contribution of the edge modes.

The DEE is found to be equivalent to the dynamical (Floquet) winding number in counting the number of emergent Floquet Majorana modes; this is discussed in appendix C.

5. DEE for periodic modulation of chemical potential in presence of spatial disorder and temporal noise

The Majorana edge-modes are robust against weak perturbations and the robustness of the Majorana modes against weak perturbations has been explored in several studies (see [77–80]). In this section, we discuss the behavior of the DEE for a periodically driven Kitaev chain in the presence of spatial disorder as well as temporal noise, and we establish that

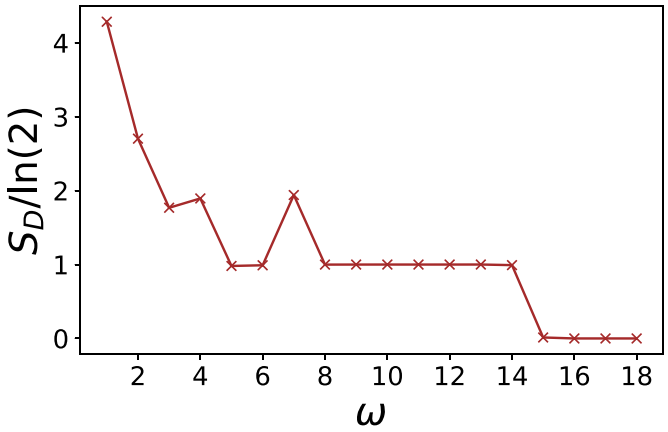

Figure 4. DEE (S_D) in units of $\ln(2)$ as a function of ω (in the units of the hopping parameter γ, which is set equal to unity) for a driving protocol in the presence of spatial disorder as given in equation (7). We have chosen $\mu_0 = 2.5$, $r = 0.2$, $\Delta = 1$, $L = 200$ and $L_D = 50$. Here, μ_0 and Δ are in the units of γ, while the parameter r is dimensionless. The dimensionless parameter β_n assumes a random value in the range $[0, 1]$. Here, S_D has been calculated after averaging over a large number of configurations of random numbers.

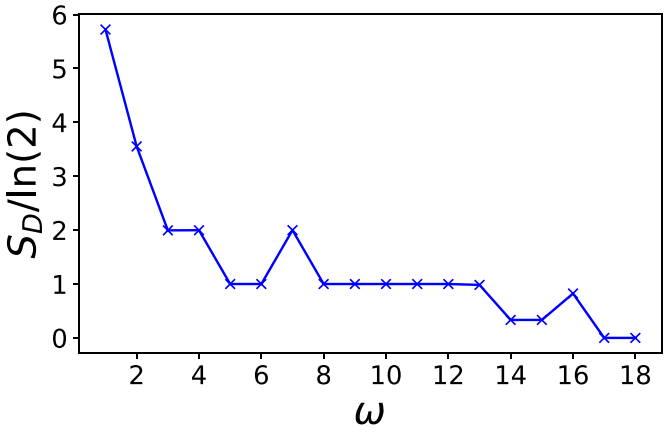

Figure 5. DEE (S_D) in units of $\ln(2)$ as a function of ω (in the units of the hopping parameter γ, which is set equal to unity) for a driving protocol in the presence of temporal noise as given in equation (8). We have chosen $\mu_0 = 2.5$, $\mu_1 = 0.2$, $r = 0.2$, $\Delta = 1$, $L = 200$ and $L_D = 50$. Here, μ_0 and Δ are in the units of γ, while the parameters μ_1 and r are dimensionless. $f(t)$ assumes a random value in the range $[-1, 1]$ in the units of γ at any time t lying in the range $[0, T]$, where $T = 2\pi/\omega$.

the Floquet Majorana modes are robust against weak spatial and temporal disorder.

5.1. DEE for periodic driving in presence of spatial disorder

We consider a driving protocol where the on-site potentials $\mu_n(t)$ for different sites are driven with δ-pulses of random amplitudes, such that the translation symmetry of the chain is explicitly broken. Therefore, we consider the following form of the chemical potential,

$$\mu_n(t) = \mu_0 + r\beta_n \sum_{m=-\infty}^{\infty} \delta(t - mT), \tag{7}$$

where n denotes the site number in the chain, μ_0 and r are independent of n, and β_n can assume a random value in the range $[0, 1]$. Here, both the parameters r and β_n are dimensionless.

After averaging over a large number of configurations of random numbers, we find that the value of the DEE, calculated in the ground state of the effective Floquet Hamiltonian, remains perfectly integer-quantized even in the presence of weak spatial disorder for high frequency (see figure 4). This demonstrates the robustness of Floquet Majorana modes (both zero and π-modes) against weak disorder. However, the deviation of the DEE from integer-quantized value at sufficiently low-frequency is due to the finiteness of the system, as we have elaborated in figure 3 for the driving protocol without spatial disorder.

5.2. DEE for periodic driving in presence of temporal noise

We now consider a driving protocol where the chemical potential $\mu(t)$ is spatially uniform, but is driven with δ-pulses in the presence of a random noise $f(t)$ of sufficiently small amplitude r. We consider the following form of the chemical potential,

$$\mu(t) = \mu_0 + \mu_1 \sum_{n=-\infty}^{\infty} \delta(t - nT) + rf(t), \tag{8}$$

where $T = 2\pi/\omega$ and the function $f(t)$ assumes a random value between $[-1, 1]$ for $0 < t < T$. Here, r is a dimensionless parameter and the value of $f(t)$ is in the units of the hopping parameter γ, where we have set $\gamma = 1$. However, we still consider the function $f(t)$ to be time-periodic with period T, i.e. $f(t) = f(t + T)$. The time-periodicity of the function $f(t)$ renders the Hamiltonian $H(t)$ periodic in time, i.e. $H(t) = H(t + T)$. We compute the DEE in the ground state of the Floquet Hamiltonian H_F for the protocol as in equation (8).

For this driving protocol with a temporal noise, we find that the value of the DEE remains invariant as shown in figure 5. This indicates the robustness of the dynamically generated Floquet Majorana modes against a weak temporal noise in the driving.

6. Detection of the anomalous edge modes with periodically modulated hopping parameter through DEE

We now consider the periodic driving of the hopping parameter γ, which may be complex in general, so that the Hamiltonian in (4) is modified to

$$H(t) = -\sum_{n=1}^{L-1} (\gamma(t) c_n^\dagger c_{n+1} + \gamma^\star(t) c_{n+1}^\dagger c_n) - \mu \sum_{n=1}^{L} (2c_n^\dagger c_n - 1) + \sum_{n=1}^{L-1} \Delta (c_n c_{n+1} + c_{n+1}^\dagger c_n^\dagger). \tag{9}$$

It has been established that for this type of driving protocol, the modes localized at the edges with the eigenvalues of the Floquet operator away from ± 1 (referred to as anomalous modes) can dynamically emerge [15]. We address here the question of whether the DEE can detect these anomalous modes.

6.1. DEE for periodic driving of the hopping parameter

We consider the following form of the hopping parameter,

$$\gamma(t) = \gamma_0 \left(1 + a\cos(\omega t)\right), \tag{10}$$

where $\omega = 2\pi/T$. Here, ω is in the units of γ_0, where we have set $\gamma_0 = 1$. The dimensionless parameter a determines the strength of the modulation of the hopping amplitude. Since the hopping parameter is chosen to be real, the time-reversal symmetry of the Hamiltonian $H(t)$ is preserved, and the periodically driven chain belongs to the BDI (Floquet) symmetry class [11, 12, 15].

To see if there are emergent anomalous modes, we plot the Floquet quasienergies θ as a function of ω for $a = 1$ in figure 6(a). Evidently, for $1.5 < \omega < 2.0$, the extreme values (near the top and bottom) of the Floquet quasienergies are separated by finite gaps from the other quasienergies. The modes with these isolated values of Floquet quasienergies are known as anomalous modes [15] since the corresponding eigenvalues of the Floquet operator differ from ± 1.

In figure 6(b), the variation of the inverse participation ratio (IPR) is plotted against the real part of the corresponding eigenvalues of the Floquet operator for $\omega = 1.7$. (For a normalized wave function $\psi_j(n)$, where j labels the wave function and n denotes the site index, the IPR is defined as $\sum_n |\psi_j(n)|^4$. It is known that as the system size L is taken to infinity, the IPRs of modes which are extended in the bulk go to zero while the IPRs of modes localized at the ends remain finite. Hence a plot of the IPR versus j provides an easy way to identify the edge modes). From this figure, it can clearly be seen that the anomalous modes (which have the minimum real part [not equal to -1] of the eigenvalues of the Floquet operator) have relatively large IPRs, compared to the other modes having non-zero Floquet quasienergies. We note here that the IPRs of the anomalous modes are almost comparable to that of the zero-energy Majorana modes (with the eigenvalue of the Floquet operator being equal to $+1$). Figure 6(c) further confirms that these anomalous modes, despite having non-zero Floquet quasienergies, are localized at the edges of the chain [15].

In figure 6(d), the DEE (S_D) is plotted as a function of the drive frequency ω to find the contribution of both the anomalous modes and the zero-energy modes to the DEE. As is evident from figure 6(d), in the approximate range of frequencies between $[1.6, 1.8]$, the non-zero and integer-quantized contribution of the anomalous modes and the zero-energy modes to the DEE enables us to detect these edge modes. In this range of frequencies, there are two anomalous modes and one Floquet zero-energy Majorana mode at each edge of the chain (one zero-energy Majorana mode at each edge is generated at $\omega = 2$ for $\gamma_0 = 1$; as the Floquet quasienergy gap closes at $\omega = 2$ for $\gamma_0 = 1$, which can be seen from the analytical calculation presented in appendix D.1) and the DEE is nearly equal to $3\ln(2)$. Further, it can be observed from figure 6(e) that the DEE converges to the value $3\ln(2)$ for sufficiently large system-size L for the drive frequency $\omega = 1.7$. Thus, we observe that $S_D/\ln(2)$ matches exactly with the number of edge modes (the zero-energy Majorana modes as well as the anomalous modes) localized at each edge for $1.6 \lesssim \omega \lesssim 1.8$. In this range of frequency, the DEE is able to detect the anomalous modes and zero-energy Majorana modes. Subsequently, we will illustrate in section 6.2 that the zero-energy Floquet Majorana modes are robust against weak spatial disorder while the anomalous modes are not.

Next, we consider a driving protocol in which the hopping parameter is complex [15], with the form

$$\gamma(t) = \gamma_0 \exp\left[ia\cos(\omega t)\right], \tag{11}$$

where $\omega = 2\pi/T$, and the parameter a determines the strength of the modulation of the phase of the hopping parameter. The complex hopping parameter in equation (11) explicitly breaks the time-reversal symmetry of the Hamiltonian $H(t)$ [12, 15]. Therefore, a chain periodically driven with this protocol belongs to the D (Floquet) symmetry class [15]. For this driving protocol, similar to the driving protocol in equation (10), zero-energy Floquet Majorana modes and anomalous modes can appear. However, we find that the DEE, calculated using the methods provided in appendix B, is not able to count the anomalous edge modes and zero-energy Majorana modes correctly for this driving protocol. In the symmetry class D, time-reversal symmetry is broken and the Majorana edge-modes are not protected from hybridization. Due to the hybridization of the edge-modes with each other (preserving particle-hole symmetry), we find that the value of $S_D/\ln(2)$ is different from the total number of Majorana modes and anomalous modes localized at each end of the chain for the symmetry class D.

6.2. Effect of spatial disorder on the DEE for periodic driving of hopping parameter

In this section, we investigate whether the dynamical zero-energy Majorana modes and the anomalous modes discussed in section 6.1 survive in the presence of weak spatial disorder. To this end, we explore the effects of disorder on the DEE for a periodic driving of the nearest-neighbor hopping amplitude.

Let us consider the driving protocol where the amplitude of the nearest-neighbor hopping parameter $\gamma_n(t)$ for the nth site is periodically modulated in the presence of spatial disorder. Therefore, this is the same driving protocol as in equation (10), but in the presence of spatial disorder. For this driving protocol, $\gamma_n(t)$ is given by,

$$\gamma_n(t) = \gamma_0(1 + a\nu_n\cos(\omega t)), \tag{12}$$

where γ_0 and the modulation strength a are independent of site index n, and the dimensionless parameter ν_n assumes random value in the range $[0, 1]$ for each site n. From figure 7, it can

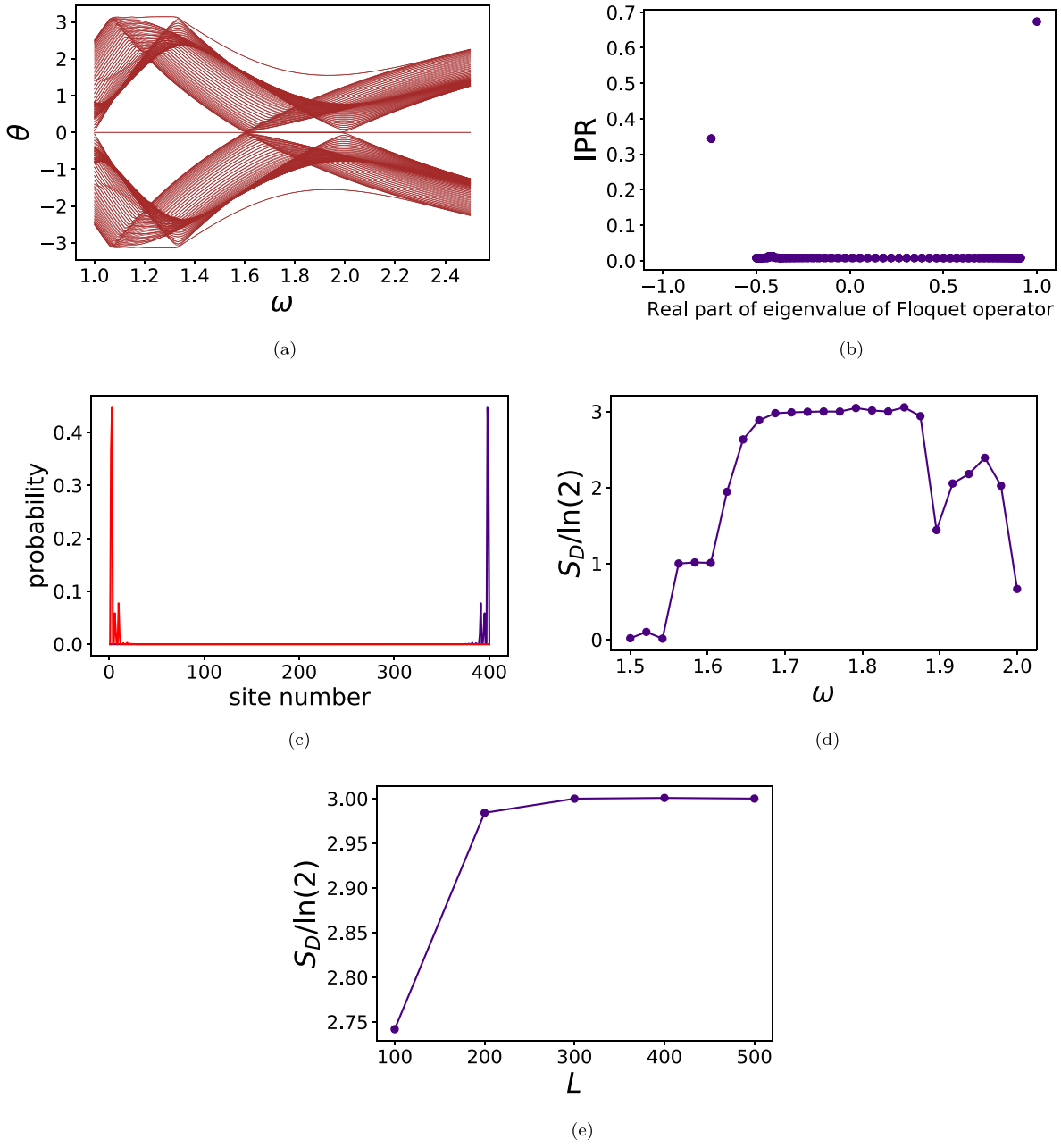

Figure 6. (a) Floquet quasienergies θ as a function of the drive frequency ω (in the units of γ_0, which is set equal to unity)). The two isolated lines seen near the top and bottom in the frequency range of about $[1.4, 2.2]$ correspond to anomalous end modes. The two isolated lines seen near the top and bottom in the frequency range of about $[1.1, 1.4]$ correspond to Majorana π modes. (b) Inverse participation ratio (IPR) as a function of the real part of the eigenvalue of the Floquet operator $U_{\rm F}$ at $\omega = 1.6$ and for $L = 200$. The modes with the real part of eigenvalue $+1$ of the Floquet operator are Majorana zero modes and the modes with the minimum real part of eigenvalue (if it is not equal to -1) of the Floquet operator are anomalous modes. There are four anomalous modes (two anomalous modes at each edge) and two zero-energy modes (one zero-energy mode at each edge). (c) Probability as a function of the site number for the two anomalous modes with the eigenvalues $-0.7412 \pm 0.6713i$ of the Floquet operator $U_{\rm F}$ at $\omega = 1.6$. (d) DEE (S_D) in units of $\ln(2)$ as a function of ω for $L = 400$ and $L_D = 100$. (e) DEE (S_D) in units of $\ln(2)$ as a function of the system-size L at $\omega = 1.7$. The DEE saturates to the value $3\ \ln(2)$ at $\omega = 1.7$ for sufficiently large L. For all the plots, the amplitude of the hopping parameter is periodically modulated (see equation (10)) with the dimensionless parameter $a = 1.0$. We have taken $\mu = 0$ and $\Delta = 0.8$; both μ and Δ are in the units of γ_0, where we have set $\gamma_0 = 1$.

clearly be seen that for $1.6 \lesssim \omega \lesssim 1.8$, the DEE is almost constant and equal to $\ln(2)$ in the presence of spatial disorder. Further, it can be observed from figure 7(b) that the DEE saturates to the value $\ln(2)$ at $\omega = 1.7$ for sufficiently large system-size L for the driving protocol in the presence of spatial disorder. On the other hand, in the absence of disorder, the DEE is equal to $3\ln(2)$ (as there are two anomalous modes and one zero-energy mode at each edge of the chain) in the same range of ω (see figure 6(d)). From this observation, we infer that the zero-energy modes remain robust against spatial disorder, whereas the anomalous edge modes disappear in the presence of spatial disorder.

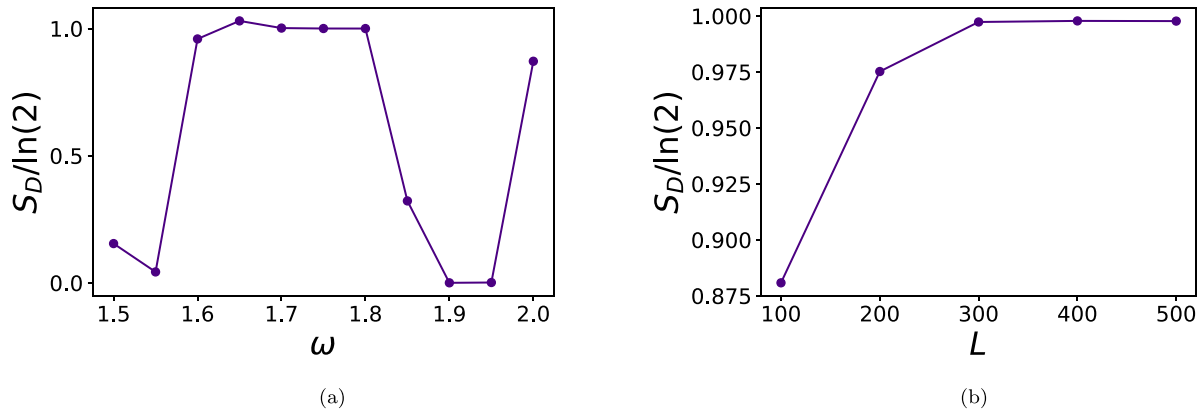

Figure 7. (a) DEE (S_D) in units of $\ln(2)$ as a function of drive frequency ω (in the units of γ_0, where $\gamma_0 = 1.0$) for periodic driving of the amplitude of the hopping parameter in the presence of spatial disorder (see equation (12)). We have taken $L = 200$, $L_D = 50$. (b) DEE (S_D) in units of $\ln(2)$ as a function of the system-size L at $\omega = 1.7$ for periodic driving of the amplitude of the hopping parameter in the presence of spatial disorder (see equation (12)). The DEE converges to the value $\ln(2)$ for sufficiently large L. For both the plots, we have taken $\Delta = 0.8$, $\mu = 0$ and $a = 1.0$. Here, μ and Δ are in the units of γ_0, while the parameter a is dimensionless. For this protocol, the dimensionless parameter ν_n assumes a random value in the range $[0, 1]$ at each site n. The DEE has been calculated after averaging over a large number of configurations of random numbers.

7. DEE for experimentally studied kicked Ising model in presence of integrability breaking interactions

In this section, we discuss a recent experimental study (see [67]) of a kicked Ising model and we thus explore the fate of the DEE in the presence of an integrability breaking perturbations.

Following [67], we consider the following driving protocol of the Hamiltonian $H_0(t) = H_0(t+T)$ of an Ising chain:

$$H_0(t) = \begin{cases} g\sum_{j=1}^{L}\sigma_j^z & \text{for} \quad 0 < t < T/2, \\ J\sum_{j=1}^{L-1}\sigma_j^x\sigma_{j+1}^x & \text{for} \quad T/2 < t < T, \end{cases} \tag{13}$$

where the σ's are Pauli matrices, g is the transverse field, and J is the coupling strength between nearest-neighbor spins. This model is integrable and can be mapped to a Kitaev chain of spinless fermions (with a driving protocol different from that we have explored in the previous sections) through Jordan–Wigner transformations [68]. The periodically driven Kitaev chain can host Floquet Majorana edge-modes. For the particular choice of the parameters $J = 0.5$ and $g = 0.6$, the first Floquet Majorana π-mode at each edge of the chain is generated at $\omega = 2.2$, as the Floquet quasienergy gap becomes $\pm\pi/T$ at $\omega = 2.2$ (see the analytical calculation presented in appendix D.2). Thus, the Floquet Majorana modes exist only for $\omega < 2.2$ for this particular choice of the parameters.

The integrability of the model can be broken by adding a longitudinal field term in the Hamiltonian $H_0(t)$. Following the driving protocol as in [67], we include a site-dependent, random longitudinal field (h_j) term (with δ-function kicks) in the Hamiltonian $H_0(t)$ to test the robustness of the Floquet Majorana modes against the integrability breaking interaction. Thus, the time-dependence of the Hamiltonian is given by

$$H(t) = H_0(t) + \frac{1}{2}\sum_{j=1}^{L} h_j\sigma_j^x \sum_{n=-\infty}^{\infty}\delta(t - nT), \tag{14}$$

where the longitudinal field h_j for the jth site is a random variable which can assume any value lying in the range $[-\pi, \pi]$, for all $j = 1, 2, \ldots, L$. Thus, the Floquet operator is given by (see also equation (1) of [67]),

$$U_F = \exp\left(-\frac{i}{2}\sum_{j=1}^{L} h_j\sigma_j^x\right)\exp\left(-i\frac{JT}{2}\sum_{j=1}^{L-1}\sigma_j^x\sigma_{j+1}^x\right) \times \exp\left(-i\frac{gT}{2}\sum_{j=1}^{L}\sigma_j^z\right). \tag{15}$$

We find that at $\omega = 2.0$ (i.e. $T = 2\pi/\omega = \pi$), the DEE (S_D) is equal to $\ln(2)$ in the integrable limit (i.e. $h_j = 0$) with parameters $J = 0.5$ and $g = 0.6$ (see the plot for $h_j = 0$ in figure 8), as there is one Floquet Majorana π-mode at each edge, namely, there are two Floquet Majorana π-modes in total at $\omega = 2.0$.

Using the exact diagonalization scheme for the non-integrable case and open boundary conditions, we find that in the presence of the random, site-dependent longitudinal field, i.e. when $h_j \neq 0$ (see figure 8), the DEE for system size $L = 4L_D = 12$ remains close to $\ln(2)$ at $\omega = 2.0$. This result indicates the robustness of the Floquet Majorana modes against an integrability breaking interaction. The deviation of the DEE from perfectly integer-quantized values at $\omega = 2.0$ in the presence of the longitudinal field is due to the finite size L of the system, as elaborated in section 4. The DEE deviates from the integer-quantized values more and more when the frequency is decreased below $\omega = 2.0$. It is also important to mention here that due to numerical limitations, the maximum size of the system for which the DEE in the non-integrable

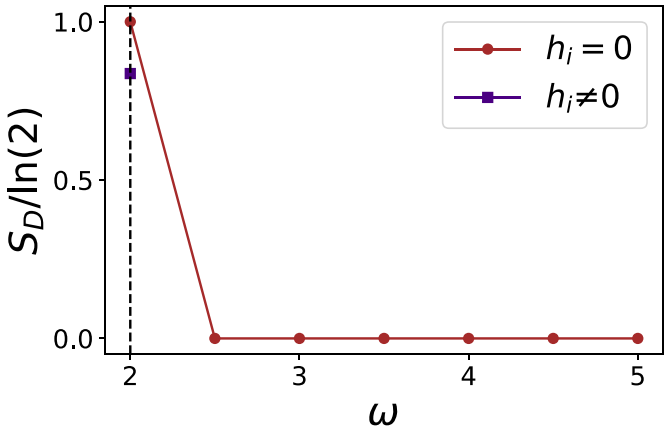

Figure 8. DEE (S_D) in units of $\ln(2)$ as a function of the drive frequency ω (in the units of J, where we have set $J = 0.5$) for the driving protocol as given in equation (14). The plot for $h_j = 0$ (the integrable case) corresponds to the driving protocol as in equation (13) with the parameters $J = 0.5$, $g = 0.6$, $L = 100$, and $L_D = L/4 = 25$. The non-integrable case with $h_j \neq 0$ corresponds to the presence of a site-dependent, random, longitudinal field in the driving, where the dimensionless parameter h_j assumes a random value between $-\pi$ and π, for all $j = 1, 2, \ldots, L$. Other relevant parameters chosen (for $h_i \neq 0$ and $\omega = 2.0$) are $J = 0.5$, $g = 0.6$, $L = 12$, and $L_D = L/4 = 3$. Here, the parameter g is in the units of J. At $\omega = 2.0$ (i.e. $T = \pi$), we observe that the DEE in the presence of a random longitudinal field and in the absence of the longitudinal field are nearly equal and close to $\ln(2)$. The deviation of the DEE from perfectly integer-quantized values in the presence of the longitudinal field is due to finite system size L, as explained in section 4.

case and open boundary conditions can be computed using the exact diagonalization scheme is given by $L = 4L_D = 12$. Thus, numerical limitations prohibit us from obtaining perfectly integer-quantized value of the DEE for the drive frequencies $\omega \leqslant 2.0$ in the presence of the integrability breaking interaction. Therefore, one cannot conclusively comment on the fate of the Floquet Majorana modes in the presence of arbitrary integrability breaking perturbations, and the results presented in figure 8 indicate their robustness at least for some values of the parameters.

8. Conclusions

In this paper, we have shown that for the periodic driving protocol of the chemical potential with δ-pulses, the DEE, calculated in the ground state of the Floquet Hamiltonian, is integer-quantized, with the integer being equal to the number of dynamically generated Floquet Majorana edge modes localized at each edge of the chain. Thus, it can be inferred that similar to the static situation, the DEE can act as a marker of Majorana edge modes even for a periodically driven Kitaev chain. At low frequencies, there is an apparent discrepancy and the value of $S_D/\ln(2)$ differs significantly from the number of Majorana end modes at each edge of the chain. However, this is an artefact of the finite size of the system, and we have established that the DEE saturates to an integer-quantized value at large system size L, even at low drive frequencies (ω of the order of the hopping amplitude γ). Thus, in a periodically driven chain with open boundary conditions, the DEE counts the number of edge Majorana modes correctly and therefore plays a role similar to that played by the winding number derived from the Floquet Hamiltonian in the corresponding system with periodic boundary conditions. Similar results can also be obtained for other periodic driving protocols (for instance, square pulse and sinusoidal modulation) of the chemical potential. Further, by probing the DEE, we have shown the robustness of the Floquet Majorana edge modes (zero modes and π-modes) against weak spatial disorder and temporal noise.

If the amplitude of the nearest-neighbor hopping in the Kitaev chain is periodically modulated (see the protocol in equation (10)), such that the Floquet Hamiltonian remains in the BDI symmetry class, then 'anomalous' edge modes (with Floquet quasienergies not equal to zero or π) can be dynamically generated. Although these anomalous edge modes do not have a topological origin and are not associated with a winding number, we find that the DEE is able to detect the existence of the anomalous edge modes for certain ranges of driving frequencies. Furthermore, we illustrate that the anomalous edge modes are not robust against weak spatial disorder, and they disappear in that situation while the zero-energy Majorana modes survive.

The dynamical generation of anomalous edge modes is also possible with the periodic modulation of the phase of the complex hopping parameter (see the driving protocol in equation (11), where the system belongs to Floquet D symmetry class). However, for this driving protocol, the DEE fails to detect them properly. Further, we have checked that one cannot infer conclusively the effects of disorder on both zero-energy and anomalous modes in the presence of spatial disorder. In the symmetry class D, time-reversal symmetry is broken and the Majorana edge-modes are not protected from hybridization. Due to the hybridization of the edge-modes with each other, we find that the value of $S_D/\ln(2)$ is different from the total number of Majorana modes and anomalous modes localized at each end of the chain for the symmetry class D. Therefore, if the edge-modes are not protected by any one (or more than one) of time-reversal symmetry, particle-hole symmetry and sub-lattice symmetry, then the value of $S_D/\ln(2)$ may differ from the number of edge-modes localized at each edge. However, it might be an interesting future work to investigate whether the DEE is able to detect the edge-modes for other symmetry classes, especially when any one of the above mentioned symmetries is not present. It might also be a possible future work to compute the DEE for systems with half-integer spins in the symmetry class CII and DIII.

We have also explored the behavior of the DEE in the presence of an integrability breaking perturbation in a kicked Ising chain, which has recently been realized experimentally [67]. However, due to numerical limitations in calculating the DEE for a sufficiently large system size in the non-integrable situation and open boundary conditions using the exact diagonalization scheme, we are unable to verify the robustness of the Floquet Majorana modes against an integrability breaking perturbation by probing the DEE.

We conclude by noting that recently the topological entanglement entropy has been measured experimentally for a two-dimensional toric code model [81]; the quantity has been measured experimentally using simulated anyon interferometry and extracting the braiding statistics of emergent excitation [81]. On the other hand, in the present work, we have computed the DEE for one-dimensional Kitaev model where anyons do not exist. We are also not aware of an equivalent of the DEE in two-dimensional situations. This experiment however provides a motivation for an experimental measurement of the DEE for one-dimensional topological systems and a possible generalization of the DEE for two-dimensional systems.

Finally, we note that it would be interesting to investigate out-of-equilibrium behavior of the DEE in Kitaev chains with more complicated couplings, like next-nearest-neighbor hopping, superconducting pairing [12, 82] and multicritical situations [83].

Data availability statement

The data that support the findings of this study are openly available at the following URL/DOI: https://doi.org/10.48550/arXiv.2203.16353.

Acknowledgment

S M acknowledges financial support from PMRF fellowship, MHRD, India. D S thanks SERB, India for funding through Project No. JBR/2020/000043. A D acknowledges support from SPARC program, MHRD, India and SERB, DST, New Delhi, India. We acknowledge Souvik Bandyopadhyay and Sourav Bhattacharjee for comments. A D acknowledges Marcello Dalmonte and Vittorio Vitale for discussion and the associateship programme, Abdus Salam ICTP, Italy.

Appendix A. Winding number and topological properties of short-range Kitaev chain

The Hamiltonian H in equation (4) of a short-range Kitaev chain with periodic boundary conditions can be written in terms the fermionic creation and annihilation operators in momentum space as

$$H = \sum_k \begin{pmatrix} c_k^\dagger & c_{-k} \end{pmatrix} H_k \begin{pmatrix} c_k \\ c_{-k}^\dagger \end{pmatrix}, \tag{A1}$$

where k lies in the range $[-\pi, \pi]$, and the Hamiltonian H_k is given by

$$H_k = (-\gamma \cos k - \mu)\, \tau_z + \Delta \sin k\, \tau_y, \tag{A2}$$

where τ_y and τ_z are Pauli matrices. In the ground state of the Hamiltonian H in equation (4), the winding number [11] is defined as

$$w = \frac{1}{2\,\pi} \int_{-\pi}^{\pi} dk \frac{d\phi_k}{dk}, \tag{A3}$$

$$\phi_k = \tan^{-1}\left(\frac{\Delta \sin k}{\gamma \cos k + \mu}\right). \tag{A4}$$

Setting the hopping parameter $\gamma = 1$, it is straightforward to check that the following phases exist in the ground state of a short-range Kitaev chain (in static situation).

(a) Topologically non-trivial phase ($-1 < \mu < 1$): this phase consists of phase I ($\Delta > 0$) and phase II ($\Delta < 0$). The winding numbers in phases I and phases II are given by $w = +1$ and $w = -1$, respectively [11]. For a chain with open boundary condition, these topologically non-trivial phases are characterized by the existence of a zero-energy Majorana mode localized at each edge of the chain [11].
(b) Topologically trivial phase ($|\mu| > 1$): the winding number is zero ($w = 0$) in this phase. For a chain with open boundary condition, Majorana edge modes do not appear in this phase.

Appendix B. Methods used for calculation of the DEE from Floquet Hamiltonian

Each fermionic creation operator $c_n^\dagger$ (or annihilation operator c_n) can be written as a linear combination of two Hermitian Majorana operators (a_{2n-1} and a_{2n}) as

$$c_n = \frac{1}{2}(a_{2n-1} - i a_{2n}), \tag{B1a}$$

$$c_n^\dagger = \frac{1}{2}(a_{2n-1} + i a_{2n}). \tag{B1b}$$

The Hamiltonian $H(t)$ of a Kitaev chain with generic time-dependent parameters can be written as,

$$H(t) = i \sum_{m=1}^{2L} \sum_{n=1}^{2L} a_m M_{mn}(t) a_n, \tag{B2}$$

where $M(t)$ is a $2L \times 2L$ real, antisymmetric matrix (which follows from the fact that Majorana operators satisfy anticommutation relations: $\{a_m, a_n\} = 2\delta_{mn}$). The $2L \times 1$ column matrix of the Majorana operators $a(t) = (a_1(t) a_2(t) \ldots a_{2L}(t))^T$ in Heisenberg picture can be written as,

$$a(t) = \mathbb{T} \exp\left(4 \int_0^t M(t')dt'\right) a(0) = U(t) a(0). \tag{B3}$$

Thus, the stroboscopic time-evolution operator (Floquet operator) is given by,

$$U_F = U(T) = \mathbb{T} \exp\left(4 \int_0^T M(t')dt'\right). \tag{B4}$$

As U_F is unitary matrix, each of its eigenvalues λ satisfies the property $|\lambda| = 1$. Thus, λ must be phases. Further, the matrix U_F is real, which ensures that the eigenvalues of U_F must appear in complex conjugate pairs, namely, $e^{i\theta}$ and $e^{-i\theta}$.

For a subsystem X with L_X fermionic sites, an element of the $2L_X \times 2L_X$ correlation matrix A_X, calculated in the ground state of the Floquet Hamiltonian, can be written as

$$(A_X)_{mn} = \langle a_m a_n \rangle. \tag{B5}$$

The von Neumann entropy S_X of the subsystem X is obtained from the eigenvalues α_j of the correlation matrix A_X as

$$S_X = -\sum_{j=1}^{2L_X} \frac{\alpha_j}{2} \ln\left(\frac{\alpha_j}{2}\right). \tag{B6}$$

S_X for $X = A, B, A \cap B$ and $A \cup B$ are calculated in the ground state of Floquet Hamiltonian and the DEE is then computed using equation (3).

Appendix C. Comparison of the DEE with the dynamical winding number for periodically driven Kitaev chain

In this section, we compare the results inferred from the behavior of the DEE with the dynamical winding number for driving protocol discussed in section 4.

For a periodically driven Kitaev chain with periodic boundary conditions, the winding number may be calculated from the stroboscopic time-evolution operator (i.e. Floquet operator)

$$U_{\rm F}(k) = \mathbb{T}\exp\left(-i\int_0^T H_k(t)dt\right) = \exp(-ih_k^{\rm F}T), \tag{C1}$$

for momentum k lying in the range $[-\pi, \pi]$, where $h_k^{\rm F}$ and $H_k(t)$ are, respectively, the Floquet Hamiltonian and the instantaneous Hamiltonian for the mode with momentum k. Referring to equation (A2), for a generic time-dependent chemical potential, we get

$$H_k(t) = (-\gamma\cos k - \mu(t))\ \tau_z + \Delta \sin k\ \tau_y. \tag{C2}$$

On the other hand, for a periodic driving, the general form of the Floquet Hamiltonian $h_k^{\rm F}$ can be written as

$$h_k^{\rm F} = d_0(k)\mathbb{1} + d_x(k)\tau_x + d_y(k)\tau_y + d_z(k)\tau_z, \tag{C3}$$

where τ_x, τ_y, τ_z are Pauli matrices and $\mathbb{1}$ is 2×2 identity matrix. Since $U_{\rm F}(k)$ is a $SU(2)$ matrix (due to the fact that $H_k(t)$ can be written as the sum of Pauli matrices with appropriate coefficients), we have $d_0(k) = 0$ for all values of k. Thus, the Floquet Hamiltonian $h_k^{\rm F}$ [11, 15] reduces to the form

$$h_k^{\rm F} = d_x(k)\tau_x + d_y(k)\tau_y + d_z(k)\tau_z. \tag{C4}$$

The coefficients d_x, d_y and d_z assume different forms for different driving protocols.

If the chemical potential is periodically modulated with δ-pulses (equation (6)), the symmetrized Floquet operator $U_{\rm F}(k)$, for k lying in the range $[-\pi, \pi]$, is given by

$$U_{\rm F}(k) = e^{i\frac{\mu_1}{2}\tau_z} e^{-iT[(-\gamma\cos k - \mu_0)\ \tau_z + \Delta \sin k\ \tau_y]} e^{i\frac{\mu_1}{2}\tau_z}. \tag{C5}$$

Since we have chosen the driving to satisfy $\mu(t) = \mu(T-t)$ and $\tau_x H_k(t)\tau_x = -H_k(T-t)$, we see that $\tau_x U_F(k)\tau_x = [U_F(k)]^\dagger)$ for all k. Using $U_{\rm F}(k) = \exp(-ih_k^{\rm F}T)$ and equation (C4), we find that $d_x(k) = 0$; we can see in figure 9(a) that this is true. We then arrive at a simplified form of the Floquet Hamiltonian $h_k^{\rm F}$

$$h_k^{\rm F} = d_y(k)\tau_y + d_z(k)\tau_z. \tag{C6}$$

This particular form of $h_k^{\rm F}$ enables us to define a dynamical winding number [11] in the following way: $d_z(k)$ is plotted as a function of $d_y(k)$ (see figures 9(b)–(d)) and the number of times the curve winds around the origin (located at $d_y = 0$, $d_z = 0$) is counted. This gives the absolute value of the Floquet winding number ($|w|$).

The Floquet winding number can also be obtained using the following method. For a generic time-dependent $\mu(t)$, the Hamiltonian H_k for k lying in the range $[0, \pi]$ is given by

$$H_k(t) = (-2\,\gamma\cos(k) - 2\mu(t))\tau_z + 2\,\Delta\sin(k)\tau_y. \tag{C7}$$

For the periodic modulation of chemical potential $\mu(t)$ with a sequence of δ-pulses as in equation (6) of the main text, the Floquet operator $U_{\rm F}(k)$ is given by

$$U_{\rm F}(k) = e^{i\mu_1\tau_z} e^{-2iT[(-\gamma\cos k - \mu_0)\ \tau_z + \Delta\sin k\ \tau_y]} e^{i\mu_1\tau_z}. \tag{C8}$$

For $k = 0$ and $k = \pi$, the Floquet operators ($U_{\rm F}(k)$) are:

$$U_{\rm F}(k=0) = \exp(i(2\,\mu_1 + 2\,T(\gamma + \mu_0))\tau_z), \tag{C9a}$$

$$U_{\rm F}(k=\pi) = \exp(i(2\,\mu_1 + 2\,T(\mu_0 - \gamma))\tau_z). \tag{C9b}$$

The Floquet operators $U_{\rm F}(k=0)$ and $U_{\rm F}(k=\pi)$ can also be written as, $U_{\rm F}(k=0) = \exp(i\pi b_0\tau_z)$ and $U_{\rm F}(k=\pi) = \exp(i\pi b_\pi\tau_z)$. Here, b_0 and b_π are given by the following equations:

$$b_0 = \frac{2\mu_1}{\pi} + \frac{4}{\omega}(\gamma + \mu_0), \tag{C10a}$$

$$b_\pi = \frac{2\mu_1}{\pi} + \frac{4}{\omega}(\mu_0 - \gamma). \tag{C10b}$$

The number of Floquet Majorana modes at each end of the chain with quasienergies zero (or eigenvalue $+1$ of the Floquet operator) and $\pm\pi/T$ (or eigenvalue -1 of the Floquet operator) are given by, $p(0) = |n_e^> - n_e^<|$ and $p(\pi/T) = |n_o^> - n_o^<|$ (as shown in [11]), where $n_e^>$ ($n_o^>$) is the number of even (odd) integers lying between b_0 and b_π, and greater than $2\mu_1/\pi$. On the other hand, $n_e^<$ ($n_o^<$) is the number of even (odd) integers lying between b_0 and b_π, and less than $2\mu_1/\pi$. The winding number [11] is determined by, $|w| = |n_e^> - n_e^< + n_o^> - n_o^<|$. Therefore, in general, we have $|w| \leqslant p(0) + p(\pi/T)$. If $p = p(0) + p(\pi/T)$ is the total number of Floquet Majorana modes at each end of the chain, then, in general, we have $|w| \leqslant p$ [11, 49]. However, if we choose $\mu_0 > \gamma$ (where $\gamma > 0$ and $\mu_0 > 0$), then for $0 < 2\mu_1/\pi < 1$, $n_o^< = n_e^< = 0$. Thus, for $0 < \mu_1 < \pi/2$, we have $p(0) = n_e^>$, $p(\pi/T) = n_o^>$ and $|w| = n_e^> + n_o^>$. Therefore, $|w| = p(0) + p(\pi/T) = p$, if $0 < \mu_1 < \pi/2$. In this

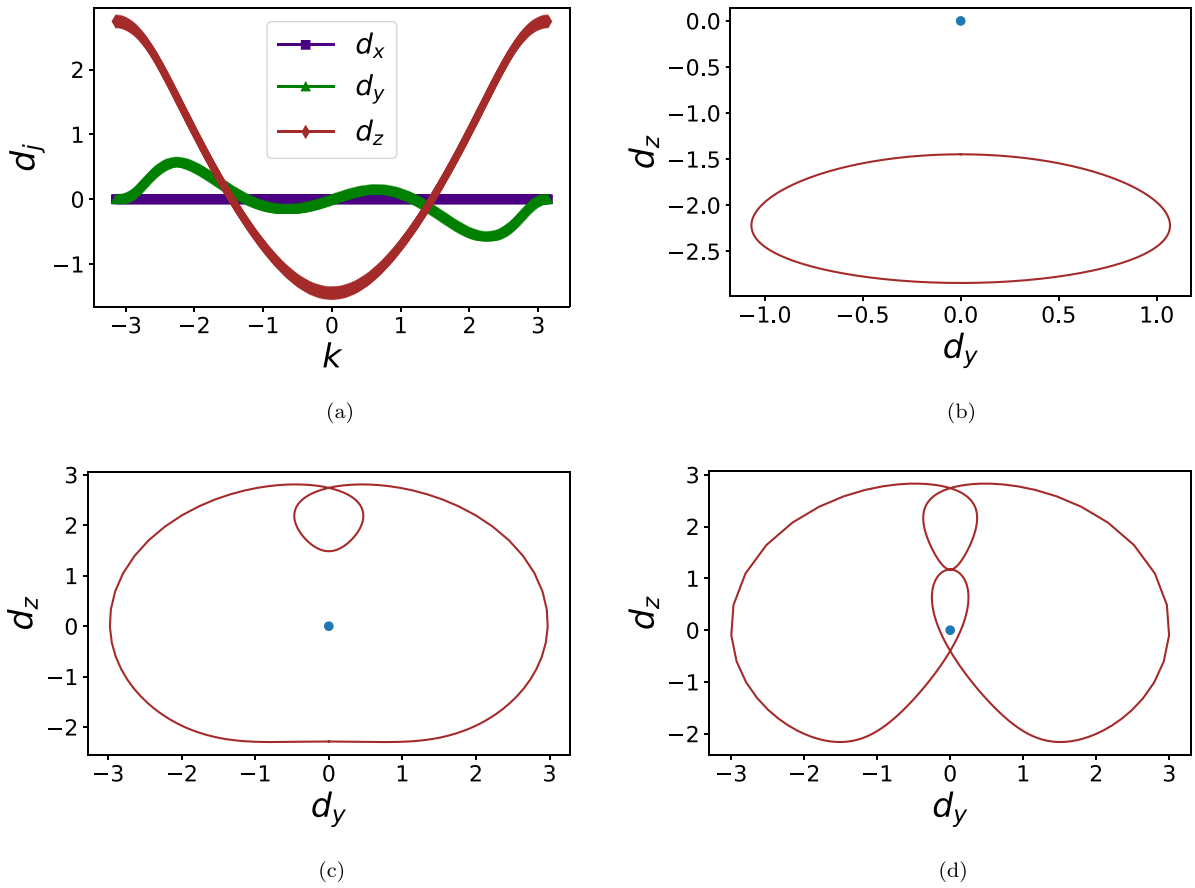

Figure 9. (a) d_x, d_y and d_z as functions of k for periodic driving of the chemical potential with a δ-pulse having $\mu_0 = 2.5$, $\mu_1 = 0.2$, and $\omega = 6.0$. We find that $d_x = 0$ for all values of k. (b) d_z as a function of d_y for $\omega = 18.0$. The dynamical (Floquet) winding number is zero. (c) d_z as a function of d_y for $\omega = 10.0$. The winding number is 1. (d) d_z as a function of d_y for $\omega = 4.0$. The winding number is 2.

situation, the winding number counts the Floquet Majorana modes (with quasienergies both zero and $\pm\pi/T$) at each end of the chain correctly. Thus, the winding number is able to characterize the topology of the Kitaev chain periodically driven with a δ-pulse.

On the other hand, the DEE, which can assume any real value, turns out to be an integer multiple of $\ln(2)$, namely, $S_D = p\ln(2)$ (see figure 2); here, the integer p is the number of Floquet Majorana modes localized at each edge (with quasienergies both zero and $\pm\pi/T$). Comparing with the Floquet winding number w, we find that $|w|\ln(2) \leqslant S_D$, in general. However, if we choose the parameters in the following way, $\gamma > 0$, $\mu_0 > 0$, $\mu_0 > \gamma$ and $0 < \mu_1 < \pi/2$, then we obtain $|w|\ln(2) = S_D$. This establishes the equivalence of the DEE with the winding number in detecting the Majorana edge modes for the periodic modulation with a δ-pulse.

Appendix D. Floquet quasienergy gap in a periodically driven chain

D.1. For periodic driving of hopping parameter

The Floquet operator for the mode with momentum k lying in the range $[0, \pi]$ is given by

$$U_{\rm F}(k) = \mathbb{T}\exp\left(-i\int_0^T H_k(t)dt\right) = \exp(-ih_k^{\rm F}T), \qquad \text{(D1)}$$

where $h_k^{\rm F}$ is the corresponding Floquet Hamiltonian. For a time-dependent hopping amplitude $\gamma(t)$, $H_k(t)$ has the form

$$H_k(t) = (-2\,\gamma(t)\cos k - 2\,\mu)\,\tau_z + 2\,\Delta\sin k\,\tau_y, \qquad \text{(D2)}$$

where $\gamma(t) = \gamma_0(1 + a\cos(\omega t))$ (see equation (10)). Using equation (D1), we obtain the following equation for $k = 0$:

$$U_{\rm F}(k=0) = e^{2iT(\gamma_0+\mu)\tau_z}. \qquad \text{(D3)}$$

For $\mu = 0$, the condition $U_{\rm F}(k=0) = \mathbb{1}$ is satisfied at the drive frequency $\omega = 2\gamma_0/n$, where n is an integer. At these frequencies, the Floquet quasienergy gap closes. Thus, the generation of zero-energy Floquet Majorana modes occurs at these specific frequencies for the driving protocol given in equation (10) in a chain with open boundary condition. For the periodic driving of the chemical potential, an analytical derivation of the frequencies at which the Floquet quasienergy gap closes can also be done by proceeding in the same way as discussed in this section (see [11]).

D.2. For the driving protocol in equation (13) for an Ising chain

Using the Jordan–Wigner transformation [68] and periodic boundary conditions for the driving protocol in equation (13) for an Ising chain, the Floquet evolution operator $U_{\rm F}(k)$ for the mode with momentum k lying in the range $[0,\pi]$ can be written as

$$U_{\rm F}(k) = e^{-i\frac{T}{2}(2J\cos(k)\tau_z - 2J\sin(k)\tau_y)} e^{-i\frac{T}{2}(2g\tau_z)}, \tag{D4}$$

where τ_y and τ_z are Pauli matrices. For the mode with momentum $k=0$, we have,

$$U_{\rm F}(k=0) = e^{-iT(J+g)\tau_z}. \tag{D5}$$

The Floquet quasienergy gap becomes zero and $\pm\pi/T$ if $U_{\rm F}(k=0) = \mathbb{1}$ and $U_{\rm F}(k=0) = -\mathbb{1}$, respectively. From these two conditions, we see that the Floquet quasienergy gap becomes zero and $\pm\pi/T$ at the drive frequencies $\omega = (J+g)/n$ and $\omega = (2J+2g)/(2n+1)$, respectively, where n is an integer. For the parameters $J=0.5$ and $g=0.6$ chosen for the numerical computations in section 7, it can be seen that the maximum values of the drive frequencies at which the Floquet quasienergy gap becomes zero and $\pm\pi/T$ are $\omega = 1.1$ and $\omega = 2.2$, respectively.

ORCID iDs

Saikat Mondal https://orcid.org/0000-0002-6954-2946
Diptiman Sen https://orcid.org/0000-0002-6926-9230
Amit Dutta https://orcid.org/0000-0002-6058-6301

References

[1] Hasan M Z and Kane C L 2010 Colloquium: topological insulators *Rev. Mod. Phys.* **82** 3045–67
[2] Qi X L and Zhang S C 2011 Topological insulators and superconductors *Rev. Mod. Phys.* **83** 1057–110
[3] Fidkowski L and Kitaev A 2011 Topological phases of fermions in one dimension *Phys. Rev.* B **83** 075103
[4] Chen X, Gu Z C, Liu Z X and Wen X G 2013 Symmetry protected topological orders and the group cohomology of their symmetry group *Phys. Rev.* B **87** 155114
[5] Senthil T 2015 Symmetry-protected topological phases of quantum matter *Annu. Rev. Condens. Matter Phys.* **6** 299–324
[6] Chiu C K, Teo J C Y, Schnyder A P and Ryu S 2016 Classification of topological quantum matter with symmetries *Rev. Mod. Phys.* **88** 035005
[7] Kitaev A Y 2001 Unpaired Majorana fermions in quantum wires *Phys.-Usp.* **44** 131–6
[8] Kitaev A and Laumann C 2009 Topological phases and quantum computation (arXiv:0904.2771)
[9] DeGottardi W, Sen D and Vishveshwara S 2011 Topological phases, Majorana modes and quench dynamics in a spin ladder system *New J. Phys.* **13** 065028
[10] DeGottardi W, Sen D and Vishveshwara S 2013 Majorana fermions in superconducting 1d systems having periodic, quasiperiodic and disordered potentials *Phys. Rev. Lett.* **110** 146404
[11] Thakurathi M, Patel A A, Sen D and Dutta A 2013 Floquet generation of Majorana end modes and topological invariants *Phys. Rev.* B **88** 155133
[12] DeGottardi W, Thakurathi M, Vishveshwara S and Sen D 2013 Majorana fermions in superconducting wires: effects of long-range hopping, broken time-reversal symmetry and potential landscapes *Phys. Rev.* B **88** 165111
[13] Rajak A and Dutta A 2014 Survival probability of an edge Majorana in a one-dimensional p-wave superconducting chain under sudden quenching of parameters *Phys. Rev.* E **89** 042125
[14] Dutta A, Aeppli G, Chakrabarti B K, Divakaran U, Rosenbaum T F and Sen D 2015 *Quantum Phase Transitions in Transverse Field Spin Models: From Statistical Physics to Quantum Information* (Cambridge: Cambridge University Press)
[15] Saha S, Sivarajan S N and Sen D 2017 Generating end modes in a superconducting wire by periodic driving of the hopping *Phys. Rev.* B **95** 174306
[16] Bandyopadhyay S, Bhattacharjee S and Dutta A 2020 Dynamical generation of Majorana edge correlations in a ramped Kitaev chain coupled to nonthermal dissipative channels *Phys. Rev.* B **101** 104307
[17] Bandyopadhyay S, Bhattacharjee S and Sen D 2021 Driven quantum many-body systems and out-of-equilibrium topology *J. Phys.: Condens. Matter* **33** 393001
[18] Russomanno A, Silva A and Santoro G E 2012 Periodic steady regime and interference in a periodically driven quantum system *Phys. Rev. Lett.* **109** 257201
[19] Tomka M, Polkovnikov A and Gritsev V 2012 Geometric phase contribution to quantum nonequilibrium many-body dynamics *Phys. Rev. Lett.* **108** 080404
[20] Nag T, Roy S, Dutta A and Sen D 2014 Dynamical localization in a chain of hard core bosons under periodic driving *Phys. Rev.* B **89** 165425
[21] Bukov M, D'Alessio L and Polkovnikov A 2015 Universal high-frequency behavior of periodically driven systems: from dynamical stabilization to Floquet engineering *Adv. Phys.* **64** 139–226
[22] Dasgupta S, Bhattacharya U and Dutta A 2015 Phase transition in the periodically pulsed Dicke model *Phys. Rev.* E **91** 052129
[23] Nag T, Sen D and Dutta A 2015 Maximum group velocity in a one-dimensional model with a sinusoidally varying staggered potential *Phys. Rev.* A **91** 063607
[24] Sen A, Nandy S and Sengupta K 2016 Entanglement generation in periodically driven integrable systems: dynamical phase transitions and steady state *Phys. Rev.* B **94** 214301
[25] Mukherjee B, Sen A, Sen D and Sengupta K 2016 Signatures and conditions for phase band crossings in periodically driven integrable systems *Phys. Rev.* B **94** 155122
[26] Eckardt A 2017 Colloquium: atomic quantum gases in periodically driven optical lattices *Rev. Mod. Phys.* **89** 011004
[27] Bhattacharya U, Maity S, Banik U and Dutta A 2018 Exact results for the Floquet coin toss for driven integrable models *Phys. Rev.* B **97** 184308
[28] Oka T and Kitamura S 2019 Floquet engineering of quantum materials *Annu. Rev. Condens. Matter Phys.* **10** 387–408
[29] Sen A, Sen D and Sengupta K 2021 Analytic approaches to periodically driven closed quantum systems: methods and applications *J. Phys.: Condens. Matter* **33** 443003
[30] Mondal S and Bhattacharjee S 2022 Periodically driven many-body quantum battery *Phys. Rev.* E **105** 044125

[31] Kitagawa T, Berg E, Rudner M and Demler E 2010 Topological characterization of periodically driven quantum systems *Phys. Rev.* B **82** 235114
[32] Jiang L, Kitagawa T, Alicea J, Akhmerov A R, Pekker D, Refael G, Cirac J I, Demler E, Lukin M D and Zoller P 2011 Majorana fermions in equilibrium and in driven cold-atom quantum wires *Phys. Rev. Lett.* **106** 220402
[33] Gu Z, Fertig H A, Arovas D P and Auerbach A 2011 Floquet spectrum and transport through an irradiated graphene ribbon *Phys. Rev. Lett.* **107** 216601
[34] Trif M and Tserkovnyak Y 2012 Resonantly tunable Majorana polariton in a microwave cavity *Phys. Rev. Lett.* **109** 257002
[35] Liu D E, Levchenko A and Baranger H U 2013 Floquet Majorana fermions for topological qubits in superconducting devices and cold-atom systems *Phys. Rev. Lett.* **111** 047002
[36] Kundu A and Seradjeh B 2013 Transport signatures of Floquet Majorana fermions in driven topological superconductors *Phys. Rev. Lett.* **111** 136402
[37] Wu C C, Sun J, Huang F J, Li Y D and Liu W M 2013 Majorana fermions in a periodically driven semiconductor-superconductor heterostructure *Europhys. Lett.* **104** 27004
[38] Tong Q J, An J H, Gong J, Luo H G and Oh C H 2013 Generating many Majorana modes via periodic driving: a superconductor model *Phys. Rev.* B **87** 201109
[39] Reynoso A A and Frustaglia D 2013 Unpaired Floquet Majorana fermions without magnetic fields *Phys. Rev.* B **87** 115420
[40] Lindner N H, Bergman D L, Refael G and Galitski V 2013 Topological Floquet spectrum in three dimensions via a two-photon resonance *Phys. Rev.* B **87** 235131
[41] Katan Y T and Podolsky D 2013 Modulated Floquet topological insulators *Phys. Rev. Lett.* **110** 016802
[42] Thakurathi M, Sengupta K and Sen D 2014 Majorana edge modes in the Kitaev model *Phys. Rev.* B **89** 235434
[43] Asbóth J K, Tarasinski B and Delplace P 2014 Chiral symmetry and bulk-boundary correspondence in periodically driven one-dimensional systems *Phys. Rev.* B **90** 125143
[44] Reichl M D and Mueller E J 2014 Floquet edge states with ultracold atoms *Phys. Rev.* A **89** 063628
[45] Perez-Piskunow P M, Foa Torres L E F and Usaj G 2015 Hierarchy of Floquet gaps and edge states for driven honeycomb lattices *Phys. Rev.* A **91** 043625
[46] Agarwala A, Bhattacharya U, Dutta A and Sen D 2016 Effects of periodic kicking on dispersion and wave packet dynamics in graphene *Phys. Rev.* B **93** 174301
[47] Roy R and Harper F 2016 Abelian Floquet symmetry-protected topological phases in one dimension *Phys. Rev.* B **94** 125105
[48] Russomanno A and Torre E G D 2016 Kibble-Zurek scaling in periodically driven quantum systems *Europhys. Lett.* **115** 30006
[49] Russomanno A, Friedman B-E and Dalla Torre E G 2017 Spin and topological order in a periodically driven spin chain *Phys. Rev.* B **96** 045422
[50] Yao S, Yan Z and Wang Z 2017 Topological invariants of Floquet systems: general formulation, special properties and Floquet topological defects *Phys. Rev.* B **96** 195303
[51] Thakurathi M, Loss D and Klinovaja J 2017 Floquet Majorana fermions and parafermions in driven Rashba nanowires *Phys. Rev.* B **95** 155407
[52] Molignini P, van Nieuwenburg E and Chitra R 2017 Sensing Floquet-Majorana fermions via heat transfer *Phys. Rev.* B **96** 125144
[53] Rodriguez-Vega M and Seradjeh B 2018 Universal fluctuations of Floquet topological invariants at low frequencies *Phys. Rev. Lett.* **121** 036402
[54] Molignini P, Chen W and Chitra R 2018 Universal quantum criticality in static and Floquet-Majorana chains *Phys. Rev.* B **98** 125129
[55] Čadež T, Mondaini R and Sacramento P D 2019 Edge and bulk localization of Floquet topological superconductors *Phys. Rev.* B **99** 014301
[56] Bhattacharya U, Maity S, Dutta A and Sen D 2019 Critical phase boundaries of static and periodically kicked long-range Kitaev chain *J. Phys.: Condens. Matter* **31** 174003
[57] Molignini P, Chitra R and Chen W 2020 Unifying topological phase transitions in non-interacting, interacting and periodically driven systems *Europhys. Lett.* **128** 36001
[58] Molignini P, Chen W and Chitra R 2020 Generating quantum multicriticality in topological insulators by periodic driving *Phys. Rev.* B **101** 165106
[59] Molignini P, Celades A G, Chitra R and Chen W 2021 Crossdimensional universality classes in static and periodically driven Kitaev models *Phys. Rev.* B **103** 184507
[60] Floquet G 1883 Sur les équations différentielles linéaires à coefficients périodiques *Ann. Sci. Ec. Norm. Super.* **12** 47–88
[61] McGinley M and Cooper N R 2018 Topology of one-dimensional quantum systems out of equilibrium *Phys. Rev. Lett.* **121** 090401
[62] Bandyopadhyay S, Bhattacharya U and Dutta A 2019 Temporal variation in the winding number due to dynamical symmetry breaking and associated transport in a driven Su-Schrieffer-Heeger chain *Phys. Rev.* B **100** 054305
[63] Bandyopadhyay S and Dutta A 2019 Dynamical preparation of a topological state and out-of-equilibrium bulk-boundary correspondence in a Su-Schrieffer-Heeger chain under periodic driving *Phys. Rev.* B **100** 144302
[64] Fromholz P, Magnifico G, Vitale V, Mendes-Santos T and Dalmonte M 2020 Entanglement topological invariants for one-dimensional topological superconductors *Phys. Rev.* B **101** 085136
[65] Micallo T, Vitale V, Dalmonte M and Fromholz P 2020 Topological entanglement properties of disconnected partitions in the Su-Schrieffer-Heeger model *SciPost Phys. Core* **3** 12
[66] Mondal S, Bandyopadhyay S, Bhattacharjee S and Dutta A 2022 Detecting topological phase transitions through entanglement between disconnected partitions in a Kitaev chain with long-range interactions *Phys. Rev.* B **105** 085106
[67] Mi X *et al* 2022 Noise-resilient Majorana edge modes on a chain of superconducting qubits (arXiv:2204.11372)
[68] Lieb E, Schultz T and Mattis D 1961 Two soluble models of an antiferromagnetic chain *Ann. Phys., NY* **16** 407–66
[69] Oshikawa M 2019 Universal finite-size gap scaling of the quantum Ising chain (arXiv:1910.06353)
[70] Peschel I 2003 Calculation of reduced density matrices from correlation functions *J. Phys. A: Math. Gen.* **36** L205–8
[71] Vidal G, Latorre J I, Rico E and Kitaev A 2003 Entanglement in quantum critical phenomena *Phys. Rev. Lett.* **90** 227902
[72] Calabrese P and Cardy J 2004 Entanglement entropy and quantum field theory *J. Stat. Mech. Theory Exp.* **2004** 06002
[73] Latorre J I and Riera A A 2009 short review on entanglement in quantum spin systems *J. Phys. A: Math. Theor.* **42** 504002
[74] Calabrese P and Cardy J 2009 Entanglement entropy and conformal field theory *J. Phys. A: Math. Theor.* **42** 504005
[75] Li Z, Zhou H, Ju C, Chen H, Zheng W, Lu D, Rong X, Duan C, Peng X and Du J 2014 Experimental realization of

a compressed quantum simulation of a 32-spin Ising chain *Phys. Rev. Lett.* **112** 220501
[76] Moore F L, Robinson J C, Bharucha C F, Sundaram B and Raizen M G 1995 Atom optics realization of the quantum δ-kicked rotor *Phys. Rev. Lett.* **75** 4598–601
[77] Hu Y, Cai Z, Baranov M A and Zoller P 2015 Majorana fermions in noisy Kitaev wires *Phys. Rev.* B **92** 165118
[78] Balabanov O and Johannesson H 2017 Robustness of symmetry-protected topological states against time-periodic perturbations *Phys. Rev.* B **96** 035149
[79] Rieder M T, Sieberer L M, Fischer M H and Fulga I C 2018 Localization counteracts decoherence in noisy Floquet topological chains *Phys. Rev. Lett.* **120** 216801
[80] Fedorova (Cherpakova) Z, Jörg C, Dauer C, Letscher F, Fleischhauer M, Eggert S, Linden S and von Freymann G 2019 Limits of topological protection under local periodic driving *Light: Sci. Appl.* **8** 63
[81] Satzinger K J *et al* 2021 Realizing topologically ordered states on a quantum processor *Science* **374** 1237–41
[82] Bhattacharjee S and Dutta A 2018 Dynamical quantum phase transitions in extended transverse Ising models *Phys. Rev.* B **97** 134306
[83] Mukherjee Victor and Dutta Amit 2010 Adiabatic multicritical quantum quenches: Continuously varying exponents depending on the direction of quenching *Europhysics Letters* **92** 37004